

Transient Run-Up Simulations of Rotors in Journal Bearings Considering Mass-Conserving Cavitation Approaches

G. Nowald, R. Schmoll, B. Schweizer

The influence of mass-conserving cavitation modeling approaches on the stability of rotors in journal bearings is investigated. The model consists of a rotor represented by a flexible multibody system and the bearings discretized with finite elements. An approach for the pressure-dependent mixture density and mixture viscosity is made. Due to this mass-conserving cavitation approach, the Reynolds equation becomes explicitly time-dependent. Both subsystems – the multibody system for the rotor and the finite element system for the bearings – are coupled by means of an explicit co-simulation approach. Two different axial boundary conditions for the bearings are considered, namely a bearing submerged in an oil bath and an oil film free to air. The differences are studied in a stationary simulation. Then, the results of transient run-up simulations of a Jeffcott rotor and a turbocharger are discussed.

1 Introduction

Rotors supported in journal bearings are nonlinear systems, which are prone to subsynchronous oscillations and oil-whirl/whip instabilities, see e.g. Khonsari and Booser (2008); Szeri (2011). Especially lightweight rotors with high rotation speeds – such as turbochargers – are characterized by subsynchronous oscillations, see for instance Schweizer (2010). Numerical run-up simulations can be used to predict and to optimize the behavior of highly nonlinear rotor systems. Usually, complex phenomena in the bearings – such as cavitation – are neglected in order to reduce calculation times.

Cavitation in dynamic journal bearings occurs due to the limited ability of fluid lubricants to support tensile stresses. The lubricant film ruptures locally, resulting in a cavity filled with gas and/or vapor, see e.g. Braun and Hannon (2010); Dowson and Taylor (1979). Simple approaches to model cavitation are the well-known half-Sommerfeld (Gümbel) or Reynolds boundary conditions, see Dowson and Taylor (1979); Khonsari and Booser (2008); Szeri (2011). These approaches yield satisfactory results under stationary conditions and high bearing loads, see e.g. Dowson and Taylor (1979), yet they do not take into account the conservation of mass.

The more sophisticated Jakobsson-Floberg-Olsson (JFO) boundary condition, ref. Floberg (1974), considers a mass-conserving 2-phase flow. This boundary condition yields a complimentary problem: In the fully developed film region, the pressure is unknown, while in the cavitated region – where the bearing gap is partially filled with gas/vapor – the fluid fraction is unknown and the pressure is assumed to be equal to ambient pressure.

The cavitation algorithm of Elrod (1981), combines two separate differential equations – one for the cavitated region and one for the fully developed fluid film – into one single equation by means of a switch function. Since the area of the cavity is not known a-priori, the switch function has to be updated repeatedly, yielding large calculation times for transient run-up simulations. Furthermore, the type of the partial differential equation changes over the spatial coordinates, which may result in numerical difficulties.

To handle the complimentary problem more efficiently, some modifications of the Elrod algorithm have been proposed. Shi and Paranjpe (2002), introduced a universal variable, which incorporates the pressure and the fluid fraction. Alakhramsing et al. (2015), replaced the switch function by Boolean expressions of the universal variable. Nitzschke et al. (2016), proposed the smoothing of the switch function to reduce the mesh solution.

In this contribution, a modified Reynolds equation introduced in ref. Nowald et al. (2016) is used to study the influence of mass-conserving cavitation on the transient dynamic behavior and the stability threshold of rotor systems. The complementary problem and the use of a switch function are avoided by introducing a pressure-dependent fluid fraction. This yields a single differential equation for the unknown pressure, which is valid for both the cavitated region and the fully developed fluid film. This enables a straightforward solution of the Reynolds equation in a FEM package, which is well suited for complicated geometries and boundary conditions, see e.g. Dahmen and Reusken (2006); Shi and Paranjpe (2002). A co-simulation scheme, see Schmoll (2015), permits a simple coupling of the bearing model with different rotor models, implemented in a multibody software. Compared to a monolithic

model, the co-simulation approach allows the modeling of the subsystems with specialized software tools.

2 Numerical Rotor-bearing Model

In this section, the numerical model used for the transient run-up simulations is described. The model consists of a rotor and a bearing model, which are coupled by means of an explicit co-simulation approach.

2.1 Rotor Model

The turbocharger shown in figure 1 is modelled in the commercial multibody software (MBS) MSC Adams. The compressor and turbine wheel are assumed rigid bodies and are connected with a flexible shaft. Unbalance masses are considered at the compressor and at the turbine wheel. The forces from the journal bearings act on the shaft as externally applied forces. The rotor is kinematically driven: the rotor-speed is linearly increased from 0 up to a rotation speed of f_{max} during the simulation time T_{sim} .

The rotor system is represented by a nonlinear differential algebraic equation system, which has the following structure, see Shabana (2013),

$$\mathbf{M}(\mathbf{q})\ddot{\mathbf{q}} = \mathbf{f}(\mathbf{q}, \dot{\mathbf{q}}, t, \mathbf{u}_{MBS}) - \mathbf{G}^T(\mathbf{q}, t)\boldsymbol{\lambda}, \quad \mathbf{0} = \mathbf{g}(\mathbf{q}, t), \quad \mathbf{y}_{MBS} = \mathbf{y}_{MBS}(\mathbf{q}, \dot{\mathbf{q}}). \quad (1)$$

In the above equation, $\mathbf{M}(\mathbf{q})$ terms the mass matrix. The vectors collecting the generalized coordinates and the generalized velocities are denoted by \mathbf{q} and $\dot{\mathbf{q}}$, respectively. The vector \mathbf{f} contains the applied, gyroscopic and elastic forces. The bearing forces/torques in the lubricant films are collected in the multibody input vector \mathbf{u}_{MBS} , which is provided by the bearing model.

The algebraic constraint equations are summarized in the vector \mathbf{g} . The resulting constraint forces are $-\mathbf{G}^T(\mathbf{q}, t)\boldsymbol{\lambda}$ with the Jacobian $\mathbf{G}^T(\mathbf{q}, t) = \partial\mathbf{g}/\partial\mathbf{q}$ and the vector of Lagrange multipliers $\boldsymbol{\lambda}$, see Shabana (2013). The term $\mathbf{y}_{MBS}(\mathbf{q}, \dot{\mathbf{q}})$ indicates the output vector of the multibody system, containing the relevant kinematical quantities for the lubricant films, which are transferred to the bearing model.

2.2 Bearing Model

The dynamic forces in the journal bearings are calculated by integration of the pressure field $p(\phi, \bar{z}, t)$ in the lubricant film, which results from the displacement and the velocity of the rotor journal with respect to the bearing shell. The compressible Reynolds equation is used for the calculation of $p(\phi, \bar{z}, t)$, see e.g. Khonsari and Booser (2008); Szeri (2011), which reads

$$\frac{\psi^2}{6} \frac{\partial}{\partial \phi} \left[\frac{\rho}{\eta} H^3 \frac{\partial p}{\partial \phi} \right] + \left(\frac{R}{B} \right)^2 \frac{\psi^2}{6} \frac{\partial}{\partial \bar{z}} \left[\frac{\rho}{\eta} H^3 \frac{\partial p}{\partial \bar{z}} \right] = \omega \frac{\partial(\rho H)}{\partial \phi} + 2 \frac{d(\rho H)}{dt}, \quad (2)$$

with the circumferential coordinate ϕ and the axial dimensionless coordinate \bar{z} . The bearing has the radius R , the axial width B and the nominal relative gap size ψ . $H(\phi, \bar{z}, t)$ is the dimensionless gap function, ω denotes the

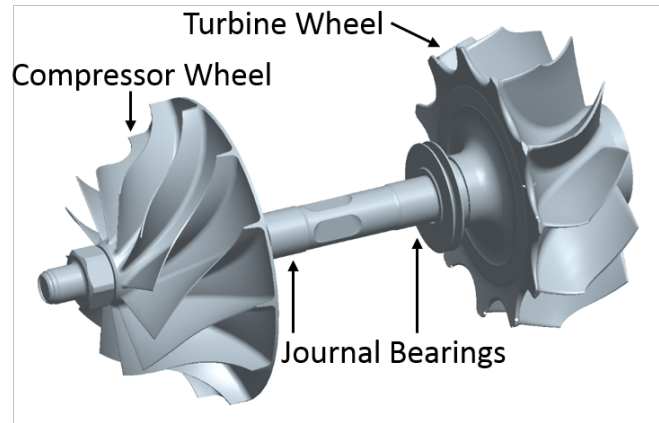


Figure 1. Turbocharger rotor

angular velocity of the rotor. ρ and η are the density and the viscosity of the lubricant, respectively.

A 2-phase cavitation approach is implemented which assumes a compressible mixture flow with mixture density ρ and mixture viscosity η . Since the mass of gas/vapor is negligible compared to the mass of the lubricant, the fluid fraction ϑ in the cavitated region is approximately equal to the density ratio, $\vartheta = \rho/\rho_0$, with the lubricant density ρ_0 , see Bartel (2010). Kumar and Booker (1991), proposed a proportional relation for the mixture viscosity

$$\vartheta = \frac{\rho}{\rho_0} = \frac{\eta}{\eta_0}, \quad (3)$$

where η_0 is the lubricant viscosity. In literature, a complementary problem is usually considered: in the fully developed film region, $\vartheta = 1$ and the pressure p is unknown, while in the cavitated film region p equals the atmospheric pressure p_0 and ϑ is unknown, see e.g. Kumar and Booker (1991); Alakhramsing et al. (2015); Nitzschke et al. (2016). In these approaches, a pressure-dependent switch function is used to determine for each discretized node separately, whether the fluid film is fully developed or cavitated.

Here, a pressure-dependent approach is made for the fluid fraction ϑ . For the fully developed fluid film, $p \geq p_0$ and $\vartheta = 1$, while for the cavitated film region $p < p_0$ and $\vartheta \rightarrow 0$. Thus, in the cavitated film region both p and ϑ can change to fulfill the Reynolds equation. A steep gradient $\partial\vartheta(p)/\partial p$ at $p \approx p_0$ causes the pressure p to only drop slightly below p_0 in the cavitated region, since the mixture density ρ is immediately reduced. A smoothed step function is used for $\vartheta(p)$, see figure 2.

Inserting equation (3) into (2) and assuming that the fluid fraction ϑ is pressure-dependent yields

$$-2H \frac{\partial\vartheta}{\partial p} \frac{dp}{dt} + \frac{\psi^2}{6\eta_0} \frac{\partial}{\partial\phi} \left[H^3 \frac{\partial p}{\partial\phi} \right] + \left(\frac{R}{B} \right)^2 \frac{\psi^2}{6\eta_0} \frac{\partial}{\partial\bar{z}} \left[H^3 \frac{\partial p}{\partial\bar{z}} \right] - \omega H \frac{\partial\vartheta}{\partial p} \frac{\partial p}{\partial\phi} = \vartheta \left[\omega \frac{\partial H}{\partial\phi} + 2 \frac{dH}{dt} \right]. \quad (4)$$

Note that equation (4) explicitly depends on time t . Since $\vartheta(p)$ is a known function, the derivative $\partial\vartheta(p)/\partial p$ can be calculated a-priori. Equation (4) is discretized with the commercial finite element software Comsol Multiphysics. The solution is stabilized by an artificial diffusion approach, see e.g. Kuzmin (2010).

The smoothing of Elrods switch function proposed in Nitzschke et al. (2016) smears the boundary between the fully developed fluid film region and the cavitated region. The smoothed switch function and the ansatz for the fluid fraction ϑ used in this contribution are both pressure-dependent and have a similar shape. However, they have different meanings: While the fluid fraction ϑ changes the compressibility of the lubricant-gas/vapor-mixture, the switch function changes the type of the differential equation. Furthermore, the switch function combines two independent differential equations for easier treatment, while equation (4) is a single differential equation for the mixture pressure, valid in both the fully developed fluid film region and the cavitated region.

For the solution of equation (4), axial boundary conditions of the pressure distribution $p(\phi, \bar{z}, t)$ in the fluid film are required. A simple and widely used assumption is constant ambient pressure p_0 , i.e.

$$p(\phi, \bar{z} = 0, t) = p(\phi, \bar{z} = 1, t) = p_0. \quad (5)$$

With the use of a Dirichlet boundary condition, the axial pressure gradient $\partial p/\partial\bar{z}$ is not specified. For classical cavitation models, the pressure p is never below ambient pressure p_0 and thus the lubricant is always flowing out of the bearing gap. Note that due to the assumption of a mixture flow, the pressure p can drop below ambient pressure

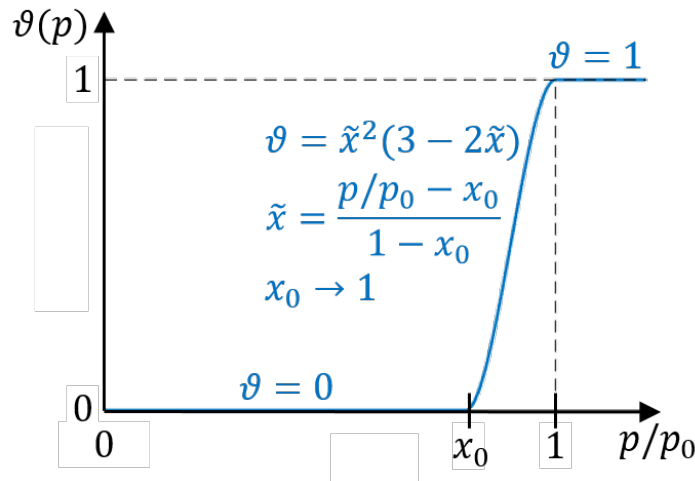


Figure 2. Pressure-dependent fluid fraction ϑ .

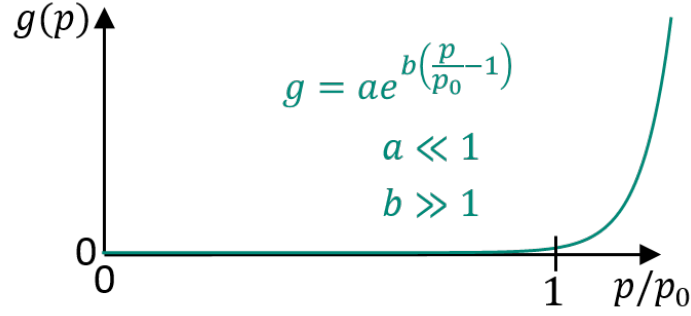


Figure 3. Penalty function $g(p)$ used for axial boundary condition (6).

p_0 , which results in a lubricant flow from the surrounding into the gap. Thus, the axial boundary condition (5) describes a bearing, which is completely submerged in an oil bath.

More common in applications of journal bearings are lubricant films, which are free to air at their axial boundaries. Here, the lubricant can only flow from the bearing gap to the surrounding. To prevent flow in the other direction, the pressure gradient $\partial p / \partial \bar{z}$ has to be 0 for $p < p_0$. This is achieved by applying a Neumann boundary condition, which incorporates a pressure dependent penalty function g :

$$\left(\frac{R}{B}\right)^2 \frac{\psi^2}{6\eta_0} \left[H^3 \frac{\partial p}{\partial \bar{z}} \right]_{\phi, \bar{z}=0, t} = g(p), \quad \left(\frac{R}{B}\right)^2 \frac{\psi^2}{6\eta_0} \left[H^3 \frac{\partial p}{\partial \bar{z}} \right]_{\phi, \bar{z}=1, t} = -g(p) \quad (6)$$

The shape of the chosen penalty function $g(p)$ is shown in Figure 3. For $p \leq p_0$, the axial flow is nearly zero, which determined by the parameter a . The flow increases sharply for $p > p_0$, which is adjusted with the parameter b . The nonlinear equation system resulting from the discretization of equation (4) is solved by an iterative Newton method. A high axial outflow lowers the pressure p at the axial boundaries of the fully developed fluid film during the solution process until $p \approx p_0$. Then the axial outflow suddenly diminishes according to Figure 3. It has been found that $a = 0.01$ and $b = 100$ yield consistent results while still enabling a stable solution.

Equation (4) cannot be solved by only defining Neumann boundary conditions. This problem is solved by incorporating an inlet boundary condition with a prescribed feeding pressure p_{inlet} , see section 3.

2.3 Co-simulation Approach

The rotor-bearing system is decomposed by means of a force/displacement coupling approach, see e.g. Schmoll (2015); Schweizer et al. (2015). The MBS and the FEM software are coupled with an in-house interface using an explicit co-simulation approach, see Schweizer et al. (2015). Since commercial solvers usually do not give the possibility to save the current solver state and to repeat a time step, more stable implicit co-simulation techniques, see e.g. Schweizer et al. (2015), cannot be used. Figure 4 shows the schematic procedure of the sequential Gauss-Seidel master-slave scheme used in this paper. For simplicity, the subsystems are shown with only one output each,

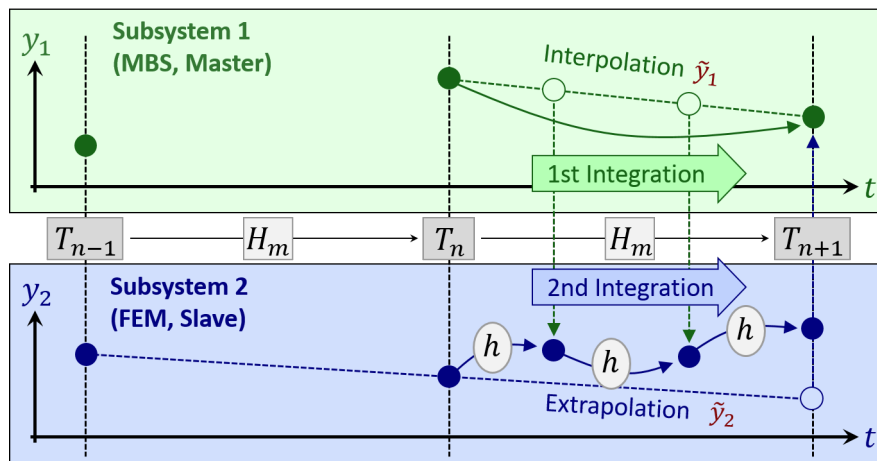


Figure 4. Explicit co-simulation approach: sequential Gauss-Seidel scheme.

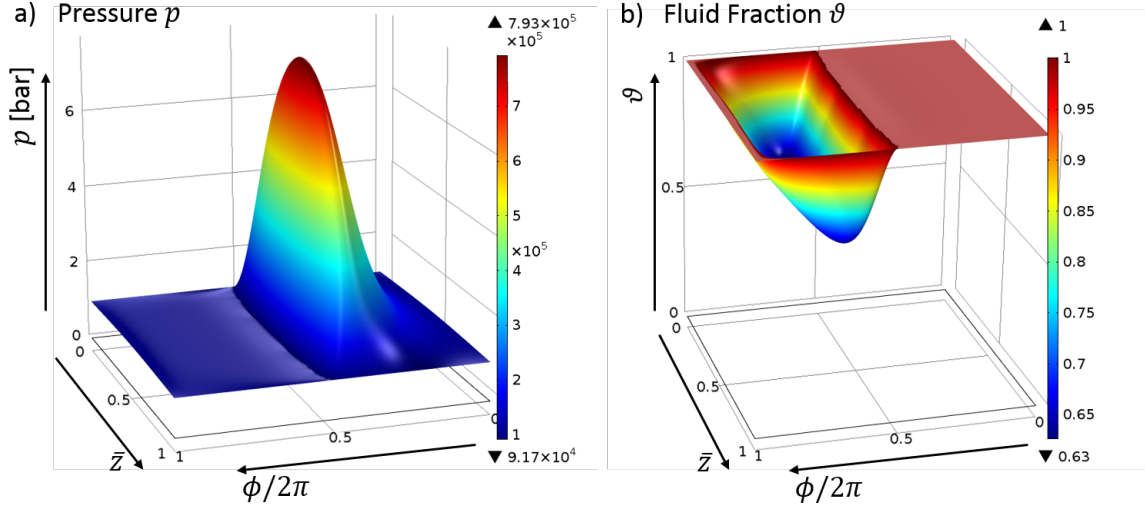


Figure 5. Stationary results for the bearing submerged in an oil bath, see eq. (5).

namely y_1 and y_2 . Firstly, subsystem 1 (master) is solved with the macro-time step H_m . At the time point T_{n+1} , the output y_2 from the second subsystem is required. Therefore, an approximation \tilde{y}_2 is carried out by applying appropriate extrapolation techniques for the output vector y_2 using the previous results. Then, subsystem 2 (slave) is solved with micro-time steps $h \leq H_m$. The required outputs y_1 from the first subsystem are approximated by the interpolation polynomial \tilde{y}_1 . Generally, Lagrange-polynomials are used for the extra- and interpolation. In this paper, both subsystems are solved using BDF-methods with variable time step size and variable integration order. In contrast to the parallel Jacobi-scheme used in Nowald et al. (2016), the subsystems have to be solved sequentially here. However, the bearing model has a substantially higher calculation time and requires smaller time steps to achieve an accurate solution, reducing the advantage of a parallel implementation. Note that the sequential Gauss-Seidel scheme usually exhibits a better stability behavior compared to the parallel Jacobi scheme, see Schmoll (2015).

3 Simulation Results

In this section, simulation results obtained with the 2-phase cavitation model are shown. Firstly, stationary calculations are performed to show the influence of the different applied axial boundary conditions. Then, results of transient run-up simulations of a Jeffcott rotor and of a heavy turbocharger with single oil films are discussed.

3.1 Influence of axial Boundary Conditions under stationary operating Conditions

Equation (4) is solved with constant kinematic input variables to study the influence of the two different axial boundary conditions (5) and (6) on the pressure distribution and the shape of the cavitated region. The shaft is considered to have a rotation speed of $\omega = 100$ Hz and a relative bearing eccentricity of $\varepsilon = 0.7$. The function H is minimal at $\phi = \pi$. The bearing parameters are $B/R = 1.6$, $\psi = 2.8\%$ and $\eta_0 = 12$ mPas. The dimensionless, developed fluid film geometry is discretized using 40×40 quadratic elements and parabolic shape functions.

Firstly, the results with the Dirichlet boundary condition (5) are shown in Figure 5. A periodic condition is used for the boundaries $\phi = 0$ and $\phi = 2\pi$, see Figure 6 a). The pressure in the fully developed fluid film region is not influenced significantly by the mass-conserving cavitation approach. Note that the ambient pressure is $p_0 = 1$ bar and that the pressure p is slightly below ambient pressure in the divergent part of the lubricant film gap. This yields a flow from the surrounding into the region of the divergent gap.

The fluid fraction ϑ represented in Figure 5 b) shows the change of the mixture properties in the lubricant film. In the convergent part of the gap, $\vartheta = 1$, i.e. the mixture density ρ and mixture viscosity η equal the properties of pure lubricant at ambient conditions, which is expected in the fully developed fluid film region. In the cavitated region, ϑ drops below 1. Since an oil bath is assumed for the axial boundary condition, the fluid fraction is 1 at the axial boundaries.

Secondly, results with the Neumann boundary condition (6) are shown in Figure 7. An axial feeding groove with an opening angle of $\theta_{\text{gap}} = 15^\circ$ is considered at $\phi = 0 = 2\pi$. A constant pressure $p_{\text{inlet}} = p_0$ is applied at the boundaries $\phi = \theta_{\text{gap}}/2$ and $\phi = 2\pi - \theta_{\text{gap}}/2$, see Figure 6 b). The pressure profile in Figure 7 a) resembles the

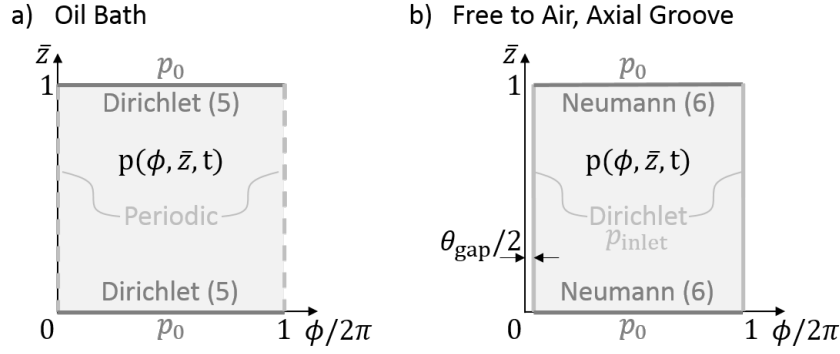


Figure 6. Pressure boundary conditions for the test cases.

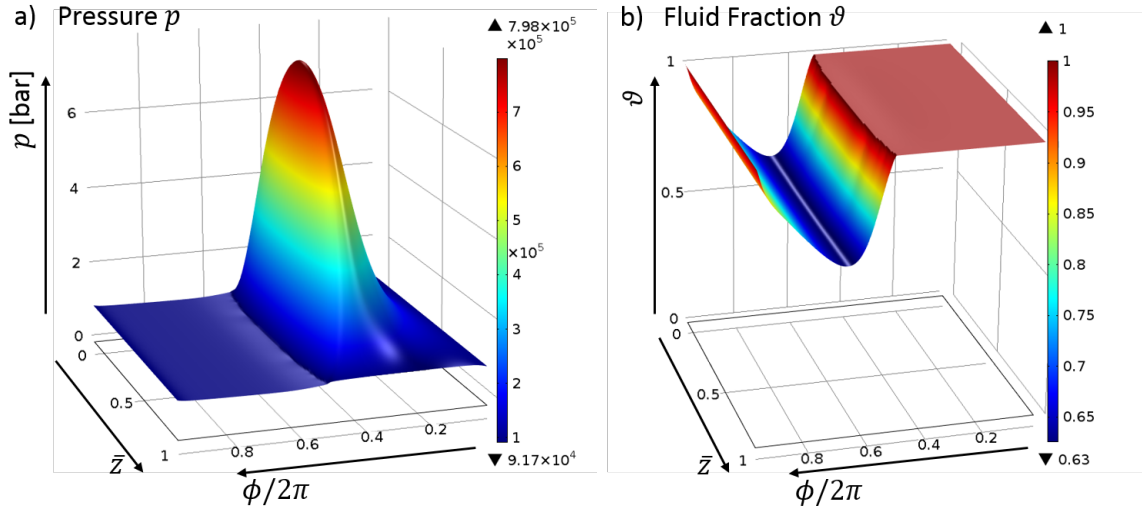


Figure 7. Stationary results for the bearing free to air, see eq. (6).

pressure distribution in Figure 5 a) in the convergent part of the gap. The difference of the maximum pressures is 0.6%. In the divergent part of the gap, the pressure also drops slightly below ambient pressure p_0 . The same minimal pressure is obtained for both boundary conditions. Note that in this case, the pressure is also below ambient pressure at the axial boundaries, resulting in a zero pressure gradient in axial direction. Hence, lubricant is not flowing at the axial boundary into the divergent part of the gap. This can also be seen in the fluid fraction ϑ shown in Figure 7 b), which also drops below 1 at the axial boundaries. The cavitated area is open to the surrounding.

3.2 Transient run-up Simulation of a Jeffcott Rotor

Transient run-up simulations of a symmetric Jeffcott rotor have been performed to study the influence of the cavitation model on the stability of the rotor-bearing system and to investigate the differences between the two different axial boundary conditions (5) and (6). The rotor has a mass of 6 kg and an unbalance of 3 gmm. The stiffness of the shaft is 4000 N/mm and the internal shaft damping is 0.1 Ns/m. External, linear viscous damping of 500 Ns/m has been applied on the center of mass of the rotor in order to enable passing through the subsynchronous oscillations. Results with low external damping have been presented in Nowald et al. (2016). The bearing parameters and the discretization are the same as in section 3.1. In the case that the bearings are free to air, axial feeding grooves with an opening angle of ϑ_{gap} and a constant feeding pressure $p_{\text{inlet}} = p_0$ are considered at the top of the bearing shells, see Figure 6 b). The rotor-speed is increased linearly from 0 to 800 Hz in 2 s.

Figure 8 shows the dimensionless eccentricity $\varepsilon(t)$ of the journal. At approximately 640 ms, the system with half-Sommerfeld cavitation boundary condition becomes unstable (oil whirl) and the journal eccentricity rises. Due to the high external damping, the eccentricity stays moderate, until the subsynchronous oscillations vanish at 1400 ms, leaving only synchronous oscillations due to unbalance.

Both simulations with the cavitation approach according to equation (4) have the onset of the oil whirl at lower rotation speeds and show higher eccentricities. The eccentricities of all three models are almost identical up to the

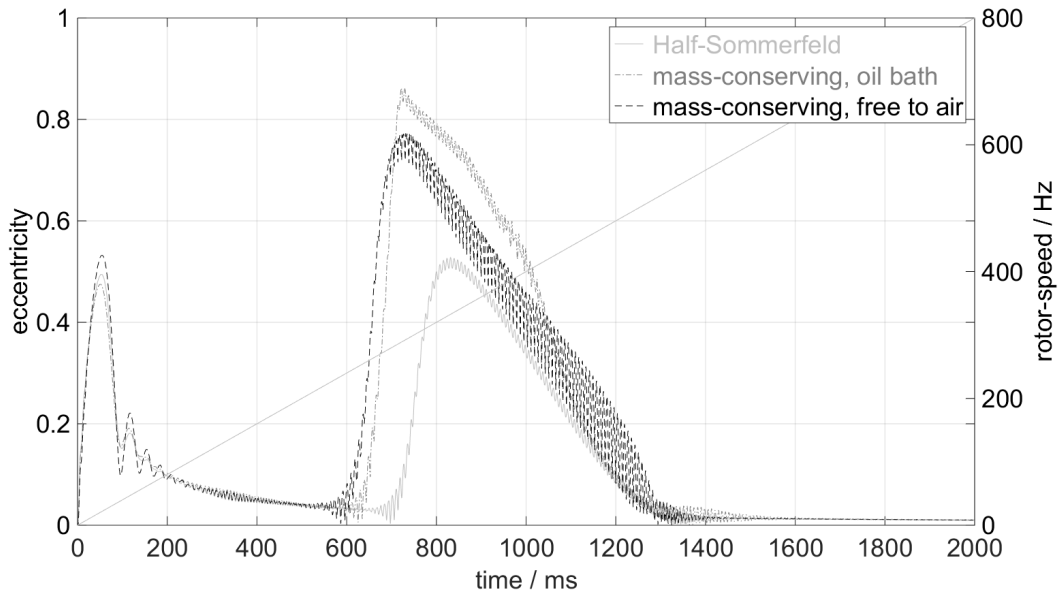


Figure 8. Run-up of a Jeffcott rotor with high external damping: journal eccentricity $\varepsilon(t)$.

onset of the oil whirl region. For all three cavitation models, the subsynchronous oscillations vanish at approximately the same rotor speed of 560 Hz.

The calculation time for one micro-step h of equation (4) using FEM discretization is approx. 10 ms on a standard desktop PC (Intel i7 processor). In the above example, the calculation time for one run-up simulation is approx. 20–30 h, depending on the number of microsteps the BDF-method takes.

3.3 Transient run-up Simulation of a Turbocharger Rotor

Now, run-up simulations with a heavy turbocharger in single oil film bearings are performed. The weight and unbalance of the rotor are the same as for the Jeffcott rotor. No external damping is applied. The bearing parameters and the discretization are equal to the corresponding parameters in the previous sections. The rotor-speed is increased linearly from 0 to 105 Hz in 7 s.

Figure 9 shows the dimensionless eccentricity $\varepsilon(t)$ of the rotor journal at the compressor-side, Figure 10 the dimensionless eccentricity $\varepsilon(t)$ at the turbine-side. Since no floating-ring bearings are considered here and no

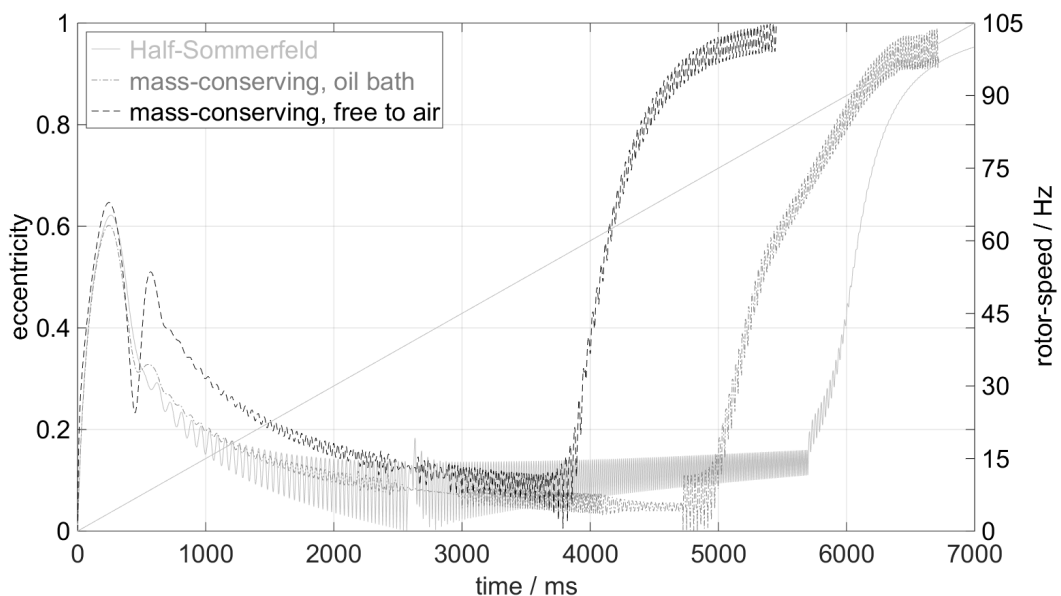


Figure 9. Run-up of a turbocharger rotor: journal eccentricity $\varepsilon(t)$ on compressor-side.

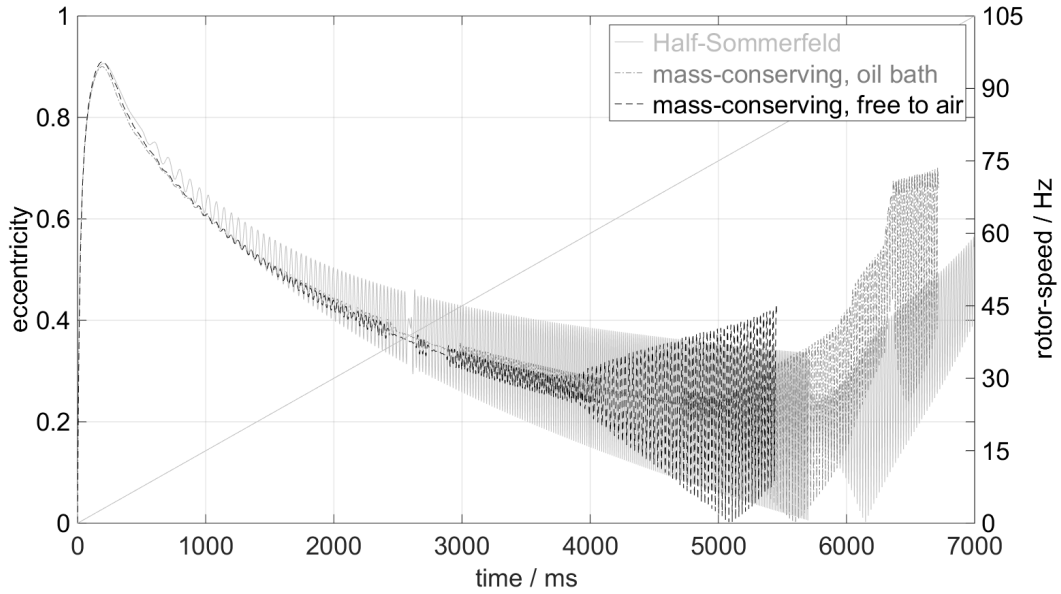


Figure 10. Run-up of a turbocharger rotor: journal eccentricity $\varepsilon(t)$ on turbine-side.

external damping is applied, the onset of the oil whirl region is reached at a low rotation speed and the eccentricities in the bearings become very large, preventing operation at higher rotation speeds. As for the Jeffcott rotor, the onset of the oil whirl is predicted at lower rotational speeds when the 2-phase cavitation approach is considered. The eccentricities of the three models are similar up to the onset of the oil whirl region. The whirl on the compressor-side is more pronounced due to the higher weight of the turbine wheel, which applies a higher load on the turbine-side journal.

4 Conclusion

In this contribution, transient run-up simulations have been performed to study the effect of mass-conserving cavitation algorithms on rotors in journal bearings. A modified Reynolds equation, which is based on a pressure-dependent density and viscosity, has been obtained. Compared to more sophisticated cavitation models, this straightforward approach can be implemented very easily within a FEM implementation. The rotor models, described as multibody systems, are coupled to the bearing model using an explicit co-simulation approach. For the axial boundary conditions of the lubricant films, two cases have been considered. It has been found that the classical prescribed pressure (Dirichlet boundary condition) corresponds to a bearing, which is completely submerged in oil. This is due to the fact that with the current cavitation approach, also pressure values below the ambient pressure are possible, resulting in a lubricant flow from the surrounding into the divergent part of the bearing gap. In many practical applications, the lubricant films are axially free to air. Thus, a second boundary condition was implemented, which makes use of a penalty function to prevent flow into the cavitated region. The two boundary conditions have been compared. While the pressure in the fully developed lubricant film is very similar for both approaches, differences in the divergent part of the bearing gap and in the shape of the cavitated area have been observed.

Finally, transient run-up simulations have been performed to study the influence of the cavitation approach on the stability of the rotor bearing system. A symmetric Jeffcott rotor and an asymmetric heavy turbocharger with single oil films have been investigated. For both rotors, the models that considered mass-conserving cavitation predicted the onset of instability at a lower rotation speed than models using the classical half-Sommerfeld cavitation approach. For rotational speeds below the threshold of instability, all three models showed good agreement with the half-Sommerfeld cavitation approach.

Current work is focused on the extension of the model to rotors in floating-ring bearings.

References

- Alakhramsing, S.; van Ostayen, R.; Eling, R.: Thermo-hydrodynamic analysis of a plain journal bearing on the basis of a new mass conserving cavitation algorithm. *Lubricants*, 3, 2, (2015), 256–280.
- Bartel, D.: *Simulation von Tribosystemen: Grundlagen und Anwendungen*. Vieweg+Teubner research, Vieweg Verlag, Friedrich & Sohn Verlagsgesellschaft mbH (2010).
- Braun, M.; Hannon, W.: Cavitation formation and modelling for fluid film bearings: a review. *Proceedings of the Institution of Mechanical Engineers, Part J: Journal of Engineering Tribology*, 224, 9, (2010), 839–863.
- Dahmen, W.; Reusken, A.: *Numerik für Ingenieure und Naturwissenschaftler*. Springer-Verlag (2006).
- Dowson, D.; Taylor, C.: Cavitation in bearings. *Annual Review of Fluid Mechanics*, 11, 1, (1979), 35–65.
- Elrod, H.: A cavitation algorithm. *Journal of Lubrication Technology*, 103, 3, (1981), 350–354.
- Floberg, L.: Cavitation boundary conditions with regard to the number of streamers and tensile strength of the liquid. *Cavitation and related phenomena in lubrication*, pages 31–36.
- Khonsari, M.; Booser, E.: *Applied Tribology: Bearing Design and Lubrication*. Tribology in Practice Series, Wiley (2008).
- Kumar, A.; Booker, J.: A finite element cavitation algorithm. *Journal of Tribology*, 113, 2-4, (1991), 276.
- Kuzmin, D.: A guide to numerical methods for transport equations. *Lecture, Friedrich-Alexander-Universität Erlangen-Nürnberg*.
- Nitzschke, S.; Woschke, E.; Schmicker, D.; Strackeljan, J.: Regularised cavitation algorithm for use in transient rotordynamic analysis. *International Journal of Mechanical Sciences*, 113, (2016), 175–183.
- Nowald, G.; Schmoll, R.; Schweizer, B.: Influence of fluid film cavitation effects on the stability of rotors in journal bearings. In: *VIRM 11 – Vibrations in Rotating Machinery, Manchester, United Kingdom, September 13th–15th* (2016).
- Schmoll, R.: *Co-Simulation und Solverkopplung: Analyse komplexer multiphysikalischer Systeme*. Ph.D. thesis, Universität Kassel (2015).
- Schweizer, B.: Dynamics and stability of turbocharger rotors. *Archive of Applied Mechanics*, 80, 9, (2010), 1017–1043.
- Schweizer, B.; Li, P.; Lu, D.: Explicit and implicit cosimulation methods: Stability and convergence analysis for different solver coupling approaches. *Journal of Computational and Nonlinear Dynamics*, 10, 5, (2015), 051007.
- Shabana, A.: *Dynamics of multibody systems*. Cambridge university press (2013).
- Shi, F.; Paranjpe, R.: An implicit finite element cavitation algorithm. *Computer Modeling in Engineering and Sciences*, 3, 4, (2002), 507–516.
- Szeri, A.: *Fluid Film Lubrication*. Cambridge University Press (2011).

Address: Institut für Angewandte Dynamik, Technische Universität Darmstadt, 64287, Darmstadt, Deutschland
email: nowald@ad.tu-darmstadt.de